Phosphine adsorption and dissociation on the Si(001) surface: An *ab initio* survey of structures

O. Warschkow,[1] H. F. Wilson,[1] N. A. Marks,[1] S. R. Schofield,[2,3] N. J. Curson,[3] P. V. Smith,[2]
M. W. Radny,[2] D. R. McKenzie,[1] and M. Y. Simmons[3]

[1]*Centre for Quantum Computer Technology, School of Physics, The University of Sydney, Sydney 2006, NSW, Australia*
[2]*School of Mathematical and Physical Sciences, The University of Newcastle, Callaghan 2308, NSW, Australia*
[3]*Centre for Quantum Computer Technology, School of Physics, University of New South Wales, Sydney 2052, NSW, Australia*

We report a comprehensive *ab initio* survey of possible dissociation intermediates of phosphine (PH_3) on the Si(001) surface. We assign three scanning tunneling microscopy (STM) features, commonly observed in room-temperature dosing experiments, to PH_2+H, PH+2H, and P+3H species, respectively, on the basis of calculated energetics and STM simulation. These assignments and a time series of STM images which shows these three STM features converting into another, allow us to outline a mechanism for the complete dissociation of phosphine on the Si(001) surface. This mechanism closes an important gap in the understanding of the doping process of semiconductor devices.

I. INTRODUCTION

Phosphine (PH_3) is a widely used molecule in the preparation of commercial *n*-type silicon wafers by chemical vapor deposition. Despite its substantial technological relevance, a detailed, atom-by-atom understanding of the PH_3 dissociation chemistry on Si(001) has remained elusive. This knowledge will become ever more critical as electronic components continue to downscale to the atomic level where devices such as single-electron transistors,[1] quantum cellular automata,[2] and quantum computers[4] become possible. Fabrication of such devices ultimately requires atomically precise placement of dopants (e.g., by scanning probe techniques) and this requires an atomistic understanding of the doping process. In the case of phosphine, such a fabrication process is illustrated by a recently proposed scheme[1,3] in which scanning tunneling microscopy (STM) hydrogen lithography is used to position individual phosphine molecules as a critical step in the fabrication of the phosphorus qubits of a silicon quantum computer.[4] Various intermediates of the dissociating PH_3 molecule are invariably encountered as prominent "features" in STM images. Only with these intermediates structurally characterized, coupled with an understanding of how they come into being and what they transform into (spontaneously or by directed manipulation), can we hope for complete control of the doping process at the atomic scale.

Although the dissociation chemistry of the PH_3/Si(001) system has been extensively studied with STM,[3,5–12] low energy electron diffraction,[13,14] desorption experiments,[14–19] many kinds of spectroscopy,[7–10,13–15,20,21] and theory,[8,20,22–25] the chemical pathways for PH_3 dissociation on the surface and subsequent P incorporation into the surface remain largely unclear. It is widely accepted that most (if not all) surface bound PH_3 dissociates into PH_2+H, however, little is known about how and under what conditions, further dissociation takes place. A widely held view is that room-temperature dissociation stops at surface bound PH_3 and PH_2 species and that further dissociation to surface bound P and subsequent incorporation into the surface requires elevated

temperatures.[15,17,20] However, this view of limited PH_3 dissociation at room temperature is not compatible with the relatively large number of intermediates observed as distinct features in STM experiments. Figure 1 shows large scale STM images of the Si(001) surface following low-dose PH_3 exposure at room temperature. Commonly observed STM features are annotated while less common PH_3-related features are indicated by circles. These images are representative samples from our extensive experimental work, the details of which will be published elsewhere.[26] The four STM features that are most commonly and consistently observed[26] following PH_3 dosing are labeled in Fig. 1 by their appearance as *asymmetric*, *centered*, *buckled*, and *U-shaped* features, respectively.

High-resolution images of these four STM features are shown in Fig. 2. In the case of the centered feature [Fig. 2(a)], no fewer than four different structural interpretations have been offered. Initially, the centered feature was assigned to a PH_3 molecule sited atop a Si-Si dimer with the P atom covalently bound to both Si atoms.[6,13] Subsequent *ab initio* calculations found this structure to be unstable.[8,20,22–25] The proposal by Kipp *et al.*[8] that the centered feature is due to a P-P dimer has been discounted by experimental observations.[7,12] Lin *et al.*[9] suggested that the feature is caused by a PH_2 group inserted into a Si-Si dimer bond. This structure is discounted in this work on energetic grounds. Finally, Miotto *et al.* attributed the centered feature to PH_2 +H bonded to opposite ends of a Si-Si dimer.[24] However, their simulated STM image was asymmetric, whereas the experimental feature [Fig. 2(a)] is centered on a dimer. The asymmetric STM feature [Fig. 2(b)] has been reported previously[5] and assigned to PH_2+H. The buckled feature shown in Fig. 2(d) has also been reported previously,[11] but remains unexplained. The U-shaped feature [Fig. 2(c)] has not been reported before. In summary, despite a great wealth of observational data, considerable ambiguity exists in the nature of these intermediates and their role in a dissociation pathway.

Using detailed quantum chemical calculations, it is our intention to bring a level of clarity to this discussion. Our
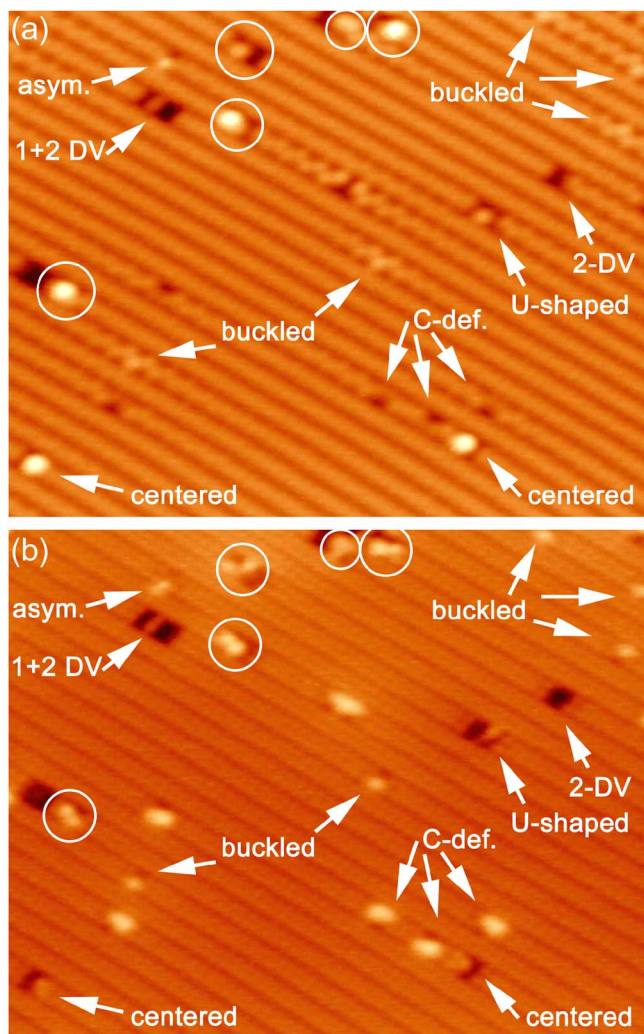
FIG. 1. (Color online) STM images in filled state (a) and empty state (b) of the Si(001) surface taken after low dose (0.001 L) PH$_3$ exposure at room temperature. Four prominently observed STM features associated with PH$_3$ dosing are labeled as *asymmetric feature*, *centered feature*, *U-shaped feature*, and the *buckled feature*. Other less common PH$_3$ related STM features are marked by circles. The 2-DV (double dimer vacancy), 1+2 DV and C-defect STM features are native defects of the Si(001) surface and are not related to PH$_3$ adsorption. Filled-state image acquired with −1.6 V, 0.1 nA. Empty-state image acquired with +1.2 V, 0.1 nA.

FIG. 2. (Color online) High-resolution filled-state and empty-state STM images of asymmetric, centered, U-shaped features, and buckled STM features commonly observed after PH$_3$ dosing of the Si(001) surface. Filled state images acquired with −1.6 V, 0.1 nA. Empty-state images acquired with +1.2 V, 0.1 nA.

us to confirm the asymmetric feature as PH$_2$+H and to assign the centered and U-shaped features as PH+2H and P+3H species, respectively. A brief account of these assignments was given by us in a recent letter.[27] In this paper we present the survey in full and elaborate on our methodology and reasoning. We present all of the candidate structures considered in our survey, discuss their physical and electronic structure, and their expected appearance in STM. Dimer pinning is presented as a tool for STM feature identification, and we outline the backbone of a dissociation and incorporation mechanism for PH$_3$ on Si(001). We further address Fourier-transform infrared (FTIR) vibrational experiments by Shan *et al.*,[20] the interpretation of which is in disagreement with our structural assignments. Calculated vibrational frequencies reported here suggest that this interpretation should be reconsidered. We note here that for reasons of scope and length, we have limited the discussion of our survey to structures in which the PH$_x$ and 3−x H remain in close proximity. This serves well as a working hypothesis as one may reasonably expect at least some (if not all) observed STM features to maintain the P+3H stoichiometry of the adsorbate. As we will show in a separate publication fragmentation does occur in some cases, leading to the *buckled* feature as well as the less-common STM features circled in Fig. 1 as fragmentation products.[26]

II. METHODS

A. Density functional methods

The survey of PH$_x$+(3−x) H structures on Si(001) was conducted using the first-principles density functional theory

primary tool in this is a rigorous *ab initio* survey of all conceivable intermediate structures of PH$_3$ dissociation; i.e., structures containing one PH$_x$ fragment (x=3,2,1,0) and 3−x H atoms bound to the surface. This provides a database of stable structures and energies, which allows us to (1) identify favorable binding sites for the PH$_x$ fragment and 3−x H atoms on the surface, and (2) establish a ranking of structures by their calculated energy (i.e., their thermodynamic stability) and their degree of dissociation (suitably captured by the number of H dissociated from PH$_3$). Structures of highest stability are thermodynamically most likely as intermediates in a dissociation path. By using STM image simulations we can match these high-stability structures with experimental STM features. As we will show below, this approach allows

(DFT) as implemented by the CPMD software.[28] The Si(001) surface was represented by a slab of five Si layers (hydrogen-terminated on one side) using a 4×4 surface unit cell which contains eight surface Si-Si dimers in two dimer rows. A single PH_3 molecule is adsorbed/dissociated per surface unit cell. Periodic images of the slab are separated by a 10Å vacuum gap. All structural parameters are fully relaxed except the deepest Si layer and the hydrogen termination, which were held fixed at free-surface positions. The DFT equations were solved in the generalized gradient approximation (GGA) using the BLYP functional[30,31] and the valence electron wave functions were expanded in a planewave basis set with a 18 Ry cutoff. The effect of core electrons was represented using Goedecker pseudopotentials[29] and **k** space was sampled at the Γ-point only.

The CPMD software is particularly economical to run in the Γ-point approximation, allowing us to perform calculations on many $PH_x + (3-x)$ H adsorbate structures using a relatively large (4×4) surface unit cell. Larger surface unit cells reduce both the interactions between periodic images of the adsorbates and the size of the irreducible Brillouin zone (IBZ); reduction of the IBZ improves the adequacy of the Γ-point approximation. The adequacy of the (4×4) cell for the purpose of our survey was tested for selected adsorbate structures using a quadruply sized (8×8) surface cell (one PH_3 molecule on 32 Si-Si dimers in four dimer rows) and relative binding energies obtained using this larger model are listed for reference alongside the (4×4) energies in the tables below. While the comparison of relative energies between the (4×4) and (8×8) models reveals differences of as much as 0.1 eV, these differences appear to be predominantly systematic in nature, exhibiting a rough correlation with the degree of dissociation and the number of dimers covered by the $PH_x + (3-x$ H) structure. Important for the following discussion is the fact that the relative energetic ordering of structures and the nature of the most stable dissociation intermediates is the same in all models considered. In the discussion below, we refer to the (4×4)-model energies unless otherwise stated.

Because we require accurately calculated vibrational frequencies in order to discuss experimental FTIR experiments,[20] we performed additional supporting calculations using the Gaussian 03 software.[32] The Gaussian software is able to compute vibrational frequencies by way of *analytical* second derivatives of the energy with respect to atomic displacements. This is important for the reliable calculation of vibrational splittings between PH stretch modes that we require in our discussion. In the Gaussian model, the surface is represented using a three-dimer $Si_{21}H_{20}$ cluster which has been variously adopted as a model for molecular adsorption and dissociation processes on Si(001).[33] The position of the cluster-terminating H atoms are held fixed in all optimizations, thus providing an *ad hoc* representation of the strain field due to surrounding Si atoms not explicitly included in the model. The nonlocal B3LYP hybrid density functional[31,34] is used, which is generally considered to deliver energies of higher accuracy than the local BLYP functional used in the CPMD slab model. The nonperiodic molecular orbitals of the cluster model are expanded in terms of

standardised basis sets of atom centered Gaussian type functions (GTF). Here we use a layered basis set expansion, with the largest (highest accuracy) atomic basis set close to the surface and a smaller, more economic basis set deeper into the surface. Using common quantum chemical notation, the basis set can be described as follows: (1) all-electron 6-311$++G(d,p)$ triple-valence zeta basis set augmented by additional polarization and diffuse functions for atoms of the PH_3 adsorbate and the first layer Si atoms; (2) all-electron 6-311$G(d)$ triple-valence zeta basis set with polarization functions for atoms of the second Si layer; and (3) pseudopotential LANL2DZ valence double zeta basis set for third and fourth layer Si atoms and cluster-terminating H atoms. Calculated energies for structures considered using the Gaussian model are listed for reference together with the CPMD results in the tables below. In order to ensure the numerical stability of the PH-stretch vibrational frequencies reported here, these were computed for structures geometry-optimized to *tight* convergence criteria using *ultrafine* exchange-correlation grids as defined by the Gaussian software.[32] Calculated frequencies are scaled by 0.971 in calibration to molecular PH-stretch modes. In order to estimate rates of reaction for two PH_3 to PH_2+H transitions, we also report below two transition states structures computed using the quadratic synchronous transit (QST3) algorithm implemented by the Gaussian software. The transition states were identified as such by the presence of a single imaginary frequency in the computed vibrational spectrum.

B. Structural survey

Since the surface reaction starts with PH_3 and ends with phosphorus incorporated into a surface dimer, we broadly classify structures in our survey into groups depending on the number of hydrogen atoms covalently bound to phosphorus. Structures in groups A, B, C, and D thus contain PH_3, PH_2+H, $PH+2H$, and $P+3H$ species, respectively. Structures in group E contain phosphorus incorporated into the top layer of the surface, with the ejected silicon atom bound to the surface as an adatom. A number of structural combinations arise for each of these sets, which differ in the relative placement of the PH_x ($x=3,2,1,0$) group and $3-x$ H atoms on the surface. We find that PH_x bonds at three sites on the Si(001) surface which gives rise to four principal bonding configurations as illustrated in Fig. 3: *dimer-end*, *dimer-bridge*, *broken-dimer*, and *end-bridge*. Broken-dimer and dimer-bridge configurations are closely related; both have the PH_x group bound centrally atop two silicon atoms of a surface dimer; however, in the broken-dimer configuration the Si-Si dimer bond is broken. H atoms generally bond only at the dimer-end position (one exception involving H in a three-center-two-electron bond is discussed in the text). Beyond the distribution of the PH_x unit and $3-x$ hydrogen atoms over available sites, further structural variations result due to (a) alternating buckling angles (see discussion below) of nearby free Si-Si dimers, and (b) different distributions of formal charge over sites. Each of these variations may result in several stable and distinct structural minima for a given placement of PH_x and $3-x$ H atoms on the surface.
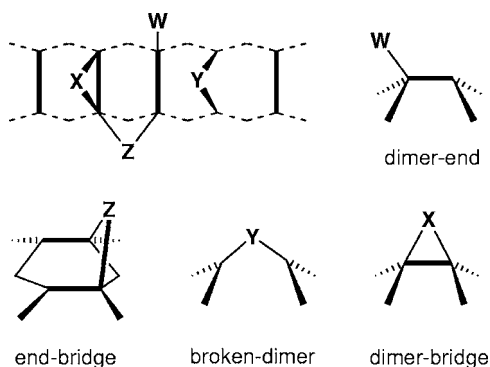
FIG. 3. Schematic top and perspective views of principal binding sites of PH_x units on the Si(001) surface. W binds in the *dimer-end* position at one end of a Si-Si surface dimer. X binds to two Si atoms of the same dimer forming a triangular *dimer-bridge* structure. Similar to a dimer-bridge, Y in a *broken-bridge* configuration, is bound to two Si atoms on the same dimer, however the Si-Si dimer bond is broken; in effect Y inserts itself into the dimer bridge. Finally, Z binds to two Si atoms of two adjacent dimers thereby bridging between two dimers in an *end-bridge* structure.

C. Valence structure diagrams

In our discussion, we make extensive use of valence structure diagrams familiar to chemists. We stress here that beyond merely showing the bond connectivity between atoms, these diagrams also provide an approximate representation of the underlying electronic structure. While certainly much simplified, a valence structure diagram attempts to capture and convey the essence of electronic bonding. Formal charges assigned to atoms in these diagrams are not to be understood as literal (i.e., partial) charges as would be obtained for example by Mulliken charge analysis; instead formal charges serve as a charge accounting device and result when electrons in formal bonds are evenly split between participating atoms. Consider, for example, a phosphorus atom which is covalently bound to four other atoms. The phosphorus atom carries a formal positive charge because all eight bonding electrons are split evenly among the bonding pairs, leaving the P atom with four electrons, one electron short of its complement of five valence electrons. Formal bonds are discerned visually from the geometry-relaxed structures via known bond lengths for single/double/triple bonds. In more complex or ambiguous cases, maximally localized WFC[35,36] were calculated from the Kohn-Sham orbitals. These provide an automated (and rigourous) partition into localized bonding-pair, lone-pair, or dangling-bond centers of electron density that can be directly translated into appropriate valence structure diagrams. This is illustrated in Fig. 4 for the PH_3-molecule attached to the Si(001) surface.

D. Si-dimer buckling and pinning

The most stable structure for the Si(001) surface at low temperature consists of an array of dimers arranged into rows,[37] with the dimers buckled at approximately 16° to the surface plane, in an alternating fashion. However, at room temperature in the absence of defects, thermal motion of the dimers causes them to flip back and forth faster than the
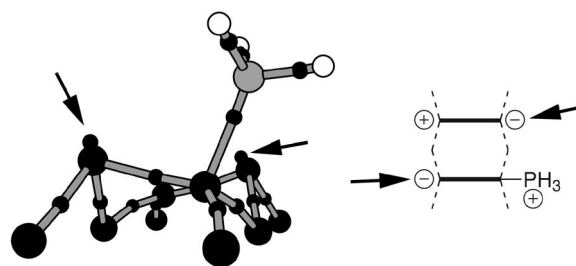
FIG. 4. Three-dimensional (3D) structural view including maximally localized Wannier function centers (WFC) and schematic valence diagram for a PH_3 molecule bound to the Si(001) surface (structure A1). P, H, and Si atoms are indicated by large grey, white, and black spheres, respectively. Wannier function centers (small black spheres) are closely related to the chemical understanding of bonding and lone-pair electrons. The arrows point to two nonbonding lone-pair WFCs on the PH_3 substituted and the buckled free dimer, leading to formal negative charges as indicated in the valence structure diagram.

STM scan time, resulting in a symmetric appearance for each dimer.[38] In the vicinity of certain surface defects, dimers are frequently observed as *pinned*, that is, locked into a single configuration for a distance of some three or four dimers away from the center (e.g., see Fig. 1).[38] This is caused by the fact that one configuration is energetically favored over the other. The extent of pinning by any particular defect may be estimated by computing the *pinning energy*[39] for that defect, corresponding to the strength of the coupling interaction between the defect and its neighboring dimers. When this pinning energy is significant relative to kT (0.025 eV at room temperature) pinning of the surrounding dimers may be expected. This is evident in filled-state STM images by an alternating buckled appearance of the dimers adjacent to a surface feature. Whether a given STM feature pins neighboring dimers or not may assist in the identification and structural characterization of the feature.

E. Simulation of STM images

For the purpose of comparing our simulated structures to real STM images, we calculate simulated STM images from our structures. Here we employ the simple yet effective Tersoff-Hamann approximation[40,41] to model the STM tunneling current. Under this approximation the tunneling current in filled/empty state is proportional to the local density of filled/empty states of the sample at the Fermi energy, $D(\mathbf{r}, E_F)$, evaluated at the point at the center of the STM tip. For filled and empty state, $D(\mathbf{r}, E_F)$ is calculated as the charge density $\rho(\mathbf{r})$ in the four nearest occupied and unoccupied states, respectively. Simulated STM images are produced in the constant-current model-showing the variation of the tip position above the surface as it follows the $3 \times 10^{-5} e/\text{Å}^3$ isosurface in $\rho(\mathbf{r})$. We have ascertained for a number of structures that the general qualitative appearance of a simulated STM image and its principal features is insensitive to changes in the number of states included in the charge summation. For the three structures that we will eventually assign to the experimental asymmetric, centered and
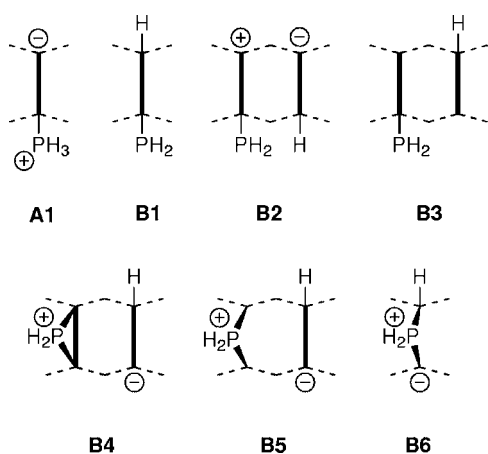
FIG. 5. Schematic view of group A and B structures involving PH_3 and PH_2 groups bound to the Si(001) surface. The formal charges assigned to atoms in these structures are as inferred from bond-valency counts for the relaxed geometry and, where ambiguous, Wannier function center analysis.

U-shaped features, the summation over four states corresponds to an energy range of ≈ 0.1 eV for filled state and ≈ 0.7 eV for empty state. These ranges are appropriate for comparison with experimental STM images taken at the low bias limit. We note that these energy ranges should not be taken as directly equivalent to the experimental bias voltage which includes additional contributions due to the voltage drop through the vacuum and surface band bending. All STM simulations are performed using the CPMD (4×4) model described above.

III. RESULTS

Our results section is organized in two parts: We will begin by surveying possible PH_3 dissociation structures in order to develop a comprehensive understanding of the relative energetics. This allows us to characterize structures in terms of stability and thus likelihood of involvement in actual dissociation processes. In the second part, we use simulated STM images to match candidate structures with experimental STM images.

A. Survey

1. Group A: Structures PH_3

Group A contains structures with a PH_3 unit chemisorbed onto the Si(001) surface. In this group, only one stable structure was found. As illustrated in Fig. 5, the structure labeled A1 contains the PH_3 group at a dimer-end position of a Si dimer. As discussed by Hamers et al.[44] PH_3 binding at this site makes sense because it combines the lone pair orbital of the phosphorus with the electron-depleted "down" atom of the Si-Si dimer. This results in a dative bond which renders the P atom fourfold coordinated and thereby formally cationic; its negative counter charge is associated with the lone-pair orbital at the up-Si atom of the dimer bridge (Fig. 4).

The A1 structure is 0.62 eV more stable than gas-phase PH_3 and the bare surface (see Table I) which is consistent

TABLE I. Energies of group A and B structures containing surface bound PH_3 as well as surface-bound PH_2 and one separate H atom. All energies are expressed in electron-volts relative to the A1 structure.

Structure		CPMD		Gaussian	Site of PH_3/PH_2
		4×4	8×8	cluster	
$PH_3(g)$		0.62	0.58	0.89	Gas-phase
PH_3	A1	0.00	0.00	0.00	Dimer-end
$PH_2 + H$	B1	−1.34	−1.30	−1.40	Dimer-end
	B2	−1.00	−1.00	−0.90	Dimer-end
	B3	−0.96	−0.86	−0.69	Dimer-end
	B4	−0.61	−0.56	−0.42	Dimer-bridge
	B5	−0.27			Broken-dimer
	B6	−0.77	−0.71		Broken-dimer

with an experimental sticking coefficient of unity. This energy is in general agreement with Miotto et al.[24] who find an adsorption energy of 0.58 eV using a smaller (2×2) simulation unit cell.

In its lowest energy configuration, structure A1 has neighboring free dimers aligned such that the negative lone pair on the substituted dimer is located next to the positive down-Si atoms on the immediately adjacent dimers on either side, i.e.,

$$(1)$$
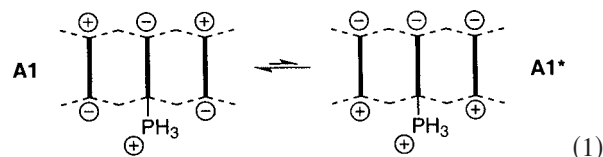
The buckling isomer A1* was found to be higher in energy by 0.22 eV, indicating a single dimer pinning energy E_p of 0.11 eV, or approximately $4kT$ at room temperature. We would thus expect this structure to show significant pinning of neighboring dimers in STM images measured at room temperature.

We also considered other binding sites for PH_3 on the surface; however, no other stable configurations were found. In these trials, the PH_3 group either relaxed to the dimer-end position or dissociated. In particular, we confirmed earlier calculations[8,20,24] that PH_3 on a dimer-bridge, proposed by Yu et al.[13] as a model for the centered feature, is not a stable structure.

2. Group B: Structures $PH_2 + H$

The most stable structure in group B is that labeled B1 in Fig. 5. This is the dissociation product discussed by Miotto et al.[23–25] with PH_2 and H bound to opposite ends of a dimer. We found B1 to be 1.34 eV more stable than A1 (see Table I), implying a strong thermodynamic driving force for dissociation. The pinning energy E_p (i.e., the energy to flip neighboring dimers) is calculated to be 0.01 eV; which indicates that B1 will not pin neighboring dimers in filled-state STM images taken at room-temperature.

The next most stable structure in group B is B2, which consists of PH_2 at a dimer-end site and the third hydrogen
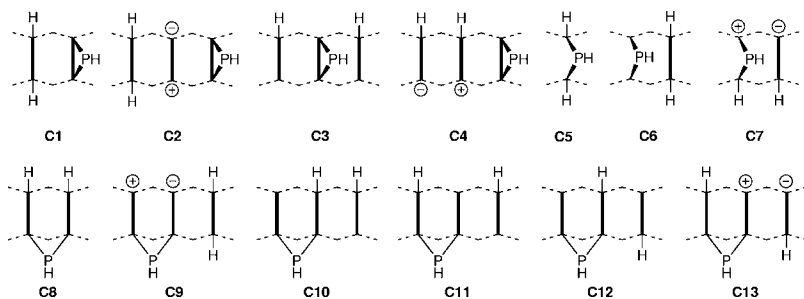
FIG. 6. Schematic diagram of structures in group C involving PH and two H atoms bound to the Si(001) surface.

attached to a neighboring dimer. B2 has the hydrogen atom attached on the same side of the dimer-row as the PH_2 group. Structure B2 is stable relative to A1 by 1.00 eV, but 0.34 eV less stable than B1. In its lowest energy charge configuration B2 is characterised by an sp^2-hybridized, formally positive Si atom on the PH_2 substituted dimer and an sp^3-hybridized, negative Si atom with a lone-pair orbital on the H-substituted dimer. The charge isomer B2*,

$$\text{B2} \quad \underset{PH_2 \quad H}{\overset{\oplus \quad \ominus}{\rule{0pt}{1em}}} \quad \rightleftharpoons \quad \underset{PH_2 \quad H}{\overset{\ominus \quad \oplus}{\rule{0pt}{1em}}} \quad \text{B2*} \qquad (2)$$
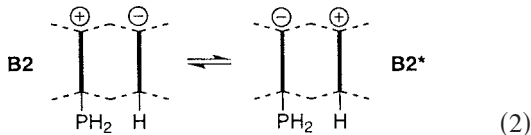
resulting from a 2*e* charge transfer from one dimer end to the other, is 0.01 eV less stable than B2, thus both configurations are expected to coexist in thermal equilibrium.

Another PH_2 dimer-end structure is B3 which has a hydrogen atom bonded to an adjacent dimer on the opposite side to the PH_2 group. This configuration is 0.38 eV less stable than the B1 structure.

In structure B4, PH_2 is bonded in a dimer-bridge site in which the PH_2 group is part of a three-membered ring and the third hydrogen atom is bound to an adjacent dimer. With four covalent bonds, the P atom carries a formal positive charge (like A1) and the negative counter-charge resides on the bare Si atom of the neighboring H-substituted dimer. This is revealed by the threefold pyramidal, sp^3-hybridized configuration of the Si atom and confirmed by WFC charge analysis.

Related to B4 is structure B5, which has PH_2 bound centrally atop a Si dimer in a broken-dimer configuration. In this structure, the Si-Si dimer bond is broken and PH_2 is effectively inserted into the dimer bond. As a result of this insertion, the two Si atoms are now threefold coordinated which leaves them with a dangling bond each. Structure B6 is also a broken-dimer structure like B5; however, it has the third hydrogen atom attached at a dimer-end position on the same dimer as the PH_2 group. This terminates one of the undercoordinated Si atoms. B6 is 0.57 eV less stable than B1.

We have also considered three different structures containing a PH_2 group in an end-bridge configuration. While converged structures were found in two instances, the geometry optimizer performed poorly in these runs, making us suspect that these structures are not true minima. Closer inspection (constrained optimizations at points displaced from these stationary points) indicates that PH_2 end-bridge structures are either transition states or very shallow minima.

Thus we do not expect PH_2 end-bridge structures as STM-observable intermediates.

3. Group C: Structures PH+2H

The set of C structures is defined by two H atom detached from PH_3, leaving a PH group and two H atoms bound to the surface. In group C, the most stable structures are C1 and C2 which are both 0.87 eV more stable than PH_2+H (structure B1). In both structures the PH group is bound at the dimer-bridge position, forming a covalent bond with both Si dimer atoms such that a three-membered ring structure results. The two detached hydrogen atoms are bound to a nearby dimer to form a *monohydride*. In the C1 structure, the monohydride is located on the dimer adjacent to the PH bridge, while in C2 the monohydride is one dimer further away. The similarity in energy of C1 and C2 attests to the fact that there is little interaction between the monohydride and the PH bridge structure. Both are closed-shell structures, have no formal charges, and do not cause pinning due to symmetry. Note that the C1 and C2 structures are far more stable than B1, meaning that after dissociation of the adsorbed PH_3 (structure A1) into PH_2+H (structure B1), the system can stabilize dramatically by further rearranging into C1.

Also more stable than B1, but less so than C1 and C2, are structures C3 and C4 in which the two detached hydrogen atoms are bound to different dimers forming a pair of *hemihydrides*. C3 has a hemihydride on either side of the PH bridge while C4 has the two hemihydrides next to each other on one side of the PH bridge. Relative to C1 and C2, structures C3 and C4 are higher in energy by 0.44 and 0.34 eV, respectively. Of the two structures, C4 is more stable, because here the hemihydrides are adjacent and therefore the unpaired electrons can pair up on one dimer to form a charged cation-anion pair as indicated in Fig. 6.

Structures C5 to C7 are broken-bridge structures: C5 is a one-dimer wide structure in which the PH group is inserted into the two Si atoms of a surface dimer and the two detached H atoms saturate the dangling bonds on the two Si atoms. Alternatively C5 can be viewed as resulting from the insertion of a divalent PH group into the two Si atoms of a monohydride. Either way, the structure is electronically closed shell and does not carry formal charges, which should be a sign of stability. C5 is considerably less stable than C1 (by 0.55 eV), but still slightly more stable than B1 (PH_2+H).

Structure C6 (not listed in Table II) is a broken-dimer PH structure with two detached hydrogens bound to a neighboring dimer as a monohydride. C6 resembles the C1 structure

TABLE II. Energies of group C dissociation products involving surface-bound PH and two additional surface-bound hydrogen atoms. All energies are in electron-volts, and are expressed relative to the A1 (adsorbed PH_3) structure.

Structure		CPMD		Gaussian	Site of PH
		4×4	8×8	cluster	
PH+2H	C1	−2.21	−2.17	−2.49	Dimer-bridge
	C2	−2.21	−2.13		Dimer-bridge
	C3	−1.77			Dimer-bridge
	C4	−1.87	−1.80		Dimer-bridge
	C5	−1.66	−1.61		Broken-dimer
	C7	−1.36			Broken-dimer
	C8	−1.78			End-bridge
	C9	−1.33			End-bridge
	C10	−1.27			End-bridge
	C11	−1.08			End-bridge
	C12	−1.31			End-bridge
	C13	−1.39			End-bridge

TABLE III. Energies of group D dissociation products of PH_3 containing one phosphorus surface adatom and three surface-bound hydrogen atoms. All energies are in electron-volts and are expressed relative to the A1 (adsorbed PH_3) structure.

Structure		CPMD		Gaussian	Site of P
		4×4	8×8	cluster	
P+3H	D1	−2.45	−2.39	−2.51	End-bridge
	D2	−2.42	−2.36	−2.51	End-bridge
	D3	−2.12		−1.76	End-bridge
	D4	−2.12		−1.88	End-bridge
	D5	−2.16	−2.13	−2.29	Dimer-bridge
	D6	−2.15	−2.09	−2.29	Dimer-bridge
	D7	−1.88			Broken-dimer
	D8	−1.84			Broken-dimer
	D9	−1.45			Broken-dimer

in which the Si-Si dimer bond is broken. While stable singlet-state minimum structures have been found in calculations using smaller (2×4) unit cells, C6 was not stable in either the CPMD (4×4) or the Gaussian cluster model.

With structures C8–C13, we consider PH end-bridge structures in which a PH group bridges between neighboring dimers. Six structures result from distinct distributions of the two H atoms over the four unterminated dimer-end sites among the two bridged dimers and the adjacent dimer. Of these structures, C8 is the most stable, but still 0.43 eV less stable than C1. Structurally, C8 is characterized by the two H atoms terminating the Si atoms on the other end of the two bridged dimers; thus leading to a two-dimer wide structure with no dangling bonds. The remaining PH end-bridge structures are significantly less stable than C8 and are therefore thermodynamically unlikely.

4. Group D: Structures P+3H

Group D contains structures in which all three hydrogen atoms are detached from the phosphorus atom. The three hydrogen atoms bind to three different Si atoms and the P atom is bound to the surface as an adatom. The survey found the P adatom is stable only in end-bridge, dimer-bridge, and broken-dimer configurations; an isolated P atom is not stable

at a dimer-end site due to the fact that such a site provides only onefold coordination. Stable structures in group D are listed in Fig. 7; calculated energies for these structures are listed in Table III.

The most stable structures in group D are the end-bridge configurations D1 and D2 which are 0.24 and 0.21 eV more stable than structure C1, respectively. In these structures, two hydrogen atoms form a monohydride on a dimer adjacent to the dimer-bridge and the third hydrogen attaches to one of the two free Si atoms opposite the phosphorus bridge. A perspective view of structure D2 is shown in Fig. 8. In this view, the bare Si atom at the center back of the structure exhibits an upwards displaced pyramidal configuration which indicates a lone pair (and thus a negative charge) at this site. We also note that the P atom at the end-bridge site forms a covalent bond with a second layer Si atom at the expense of one of the Si-Si backbonds. This is evident in the bondlengths in Fig. 8 where the Si-P bond is of normal length (2.31 Å), whereas one of the two backbonds is elongated to 2.56 Å from typically 2.38 Å. Structures D1 and D2 differ only in the placement of the third hydrogen atom relative to the monohydride dimer but otherwise share many structural details. In particular, the lengthening of the Si-Si backbond is also observed in the D1 structure.

Structures D3 and D4 are also end-bridge P structures in which both of the dimer-end sites opposite the P bridge are terminated by H atoms. The third hydrogen atom is bound to a third, adjacent dimer. D3 and D4 are less stable than D1 by
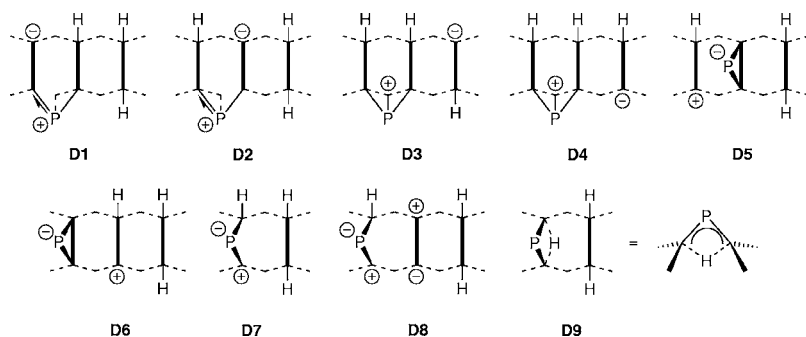
FIG. 7. Schematic diagram of structures in group D involving P and three H atoms bound to the Si(001) surface.
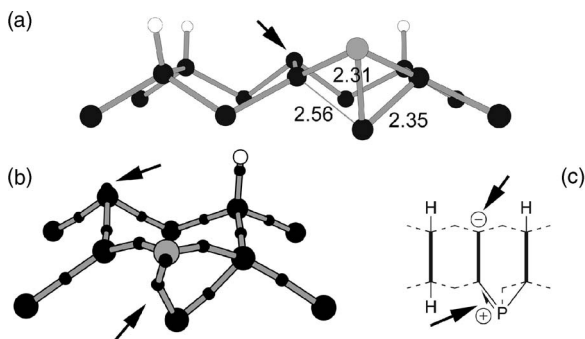
FIG. 8. Structure D2 represented by (a) ball-and-stick model. (b) Wannier function center view, and (c) schematic valence bonding diagram. P, H, and Si atoms are indicated by grey, white and large black spheres, respectively. WFC are indicated by small black spheres. The bond lengths (given in Å) illustrate the lengthening of a Si backbond. The Wannier function analysis (b) reveals a lone pair and thus a negative charge on the center back Si atom.

0.33 eV, which can be attributed to the stable monohydride unit present in D1 and D2 but absent in D3 and D4. Structures D5 and D6 contain P in a dimer-bridge position, with the three hydrogen atoms distributed over the two neighboring dimers, forming a monohydride and a hemihydride dimer in each case. D5 and D6 are less stable than D1 by 0.29 and 0.30 eV, respectively, which (like D3 and D4) brings them into close energetic proximity with C1 (but still less stable by ≈ 0.05 eV). Structure D5 in particular appears readily accessible from structure C1 by a proton shift to an adjacent (buckled) dimer, i.e.,

$$(3)$$
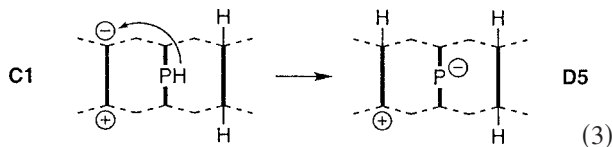
which makes D5 a conceivable, if transient, intermediate in any onward reaction from C1. We will return to this particular process in the discussion section below.

Structures D7 and D8 are broken-dimer structures with one dangling bond terminated by a hydrogen atom; the two remaining H atoms form a monohydride on a nearby dimer. Structures D7 and D8 are 0.57 and 0.61 eV less stable than the end-bridge structure D1. Notably, both D7 and D8 have the nonterminated Si atom in the broken-dimer bridge in a nearly threefold planar coordination (i.e., sp^2-hybridized). This is consistent with a cationic charge on this site and thus two lone-pair orbitals on the twofold coordinated P atom provide the negative countercharge.

Finally, structure D9 is an unusual structure inspired by a similar structure reported in the survey of gas-phase Si_2PH_x structures of Wittbrodt *et al.*[42] This structure consists of a P atom at a broken-dimer site and two hydrogen atoms bound as a monohydride on the neighboring dimer. The third hydrogen atom is held in between the two broken-dimer Si atoms and below the bridging P atom in a two-electron, three-center bond. The D9 structure is related to structure C1 via a proton shift, but is 0.76 eV less stable and thus unlikely to be observed.
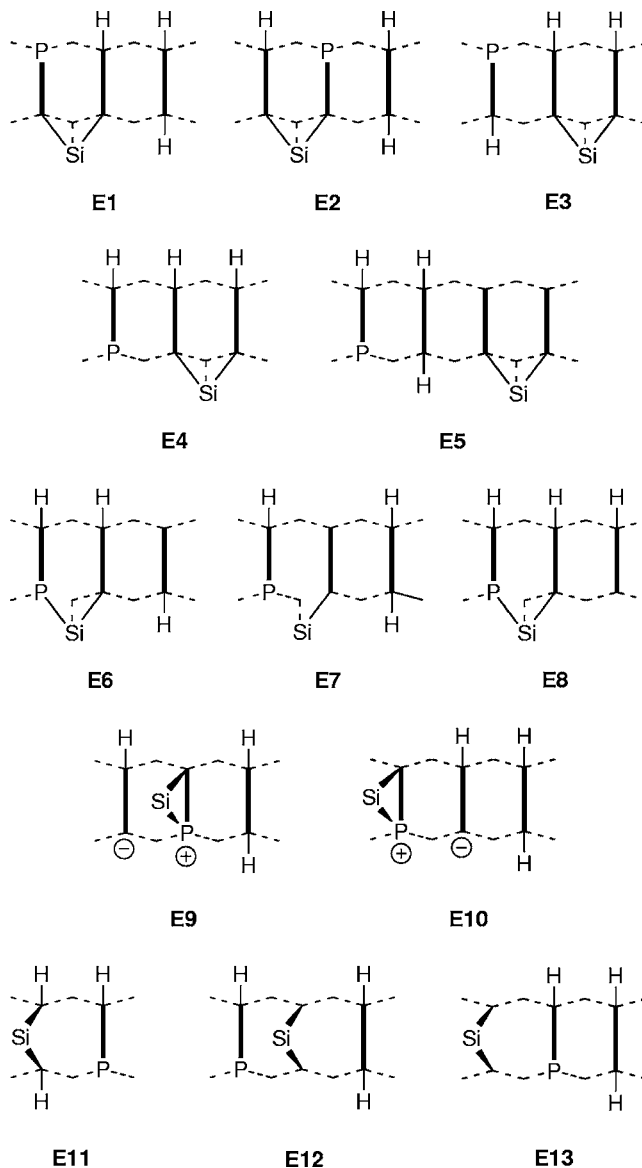
FIG. 9. Schematic view of group E structures involving phosphorus incorporated into the surface as a heterodimer, three surface bound hydrogen atoms, and a silicon adatom.

5. Group E: Heterodimer+Si+3H

STM experiments have shown that thermal annealing of the phosphine doped surface at elevated temperatures (650 K) yields P atoms incorporated into the surface as *heterodimers*.[6,12] This is evidenced by the formation of Si adatoms ejected from the dimer during P incorporation. With the set of group E structures (Fig. 9), we consider various combinations of a surface incorporated P atom, three surface bound H atoms and a Si adatom. We point out that the set of group E structures is less comprehensive than the other groups due to the permutational complexity added by the placement of the P atom relative to the surface bound Si and H atoms. The objective of the group E survey is primarily to explore typical binding sites and illustrate the energetics of P incorporation, rather than to give a complete picture of all possible structures in the PH_3 stoichiometry with an incorporated phosphorus atom.

TABLE IV. Energies of group E dissociation products containing a surface incorporated P atom (heterodimer), a Si surface adatom, and three surface-bound hydrogen atoms. All energies are in electron-volts relative to the A1 (adsorbed PH_3) structure.

Structure		CPMD		Gaussian	Site of Si
		4×4	8×8	cluster	
Si+3H	E1	−2.91	−2.80	−3.35	End-bridge
	E2	−2.91	−2.81		End-bridge
	E3	−2.84			End-bridge
	E4	−2.82	−2.73		End-bridge
	E5	−2.45			End-bridge
	E6	−1.87			End-bridge
	E7	−1.82			End-bridge
	E8	−2.10			End-bridge
	E9	−2.00			Dimer-bridge
	E10	−1.99			Dimer-bridge
	E11	−1.67			Broken-dimer
	E12	−2.53			Broken-dimer
	E13	−2.50			Broken-dimer

The lowest energy structures found in group E (see Table IV) are E1 and E2 which are both 0.46 eV more stable than structure D1, showing that phosphorus incorporation results in a substantial energy gain. E1 and E2 consist of a heterodimer with the Si adatom at an end-bridge site linking the heterodimer on the Si side to an adjacent dimer. This second dimer is H terminated on the other end and the two remaining H atoms form a monohydride structure on a neighboring third dimer. E1 and E2 differ only in the placement of the monohydride dimer relative to the phosphorus atom. Chemically, E1 and E2 are isoelectronic to structures D1 and D2, respectively.

Structures E3 and E4 are also quite stable, being only 0.07 and 0.09 eV less stable than E1 and E2, and therefore more stable than D1 and D2. Both E3 and E4 contain a *hydrogenated heterodimer* structure as well as Si bound at an end-bridge site, with the bridged dimers saturated on the other side by the two remaining H atoms.

Structure E5 contains a monohydride and a hydrogenated heterodimer, as well as the Si adatom at an end-bridge on two separate dimers. Structure E5 is found to be 0.46 eV less stable than E1. While both the hydrogenated heterodimer and the monohydride are closed-shell structures, this stability is offset by the open-shell structure created by the Si atom on the other two dimers.

E6–E8 are all open-shell end-bridge structures in which the Si adatom binds directly to the phosphorus atom. These are high-energy structures of between +0.81 and +1.09 eV relative to E1. Similar energies (+0.91 and +0.92 eV) are found for structures E9 and E10 which also have the Si adatom bound directly to phosphorus but located on a dimer-bridge site.

Finally, structures E11 to E13 have the Si adatom located on a broken-dimer site. All three structures contain a monohydride, a hydrogenated heterodimer and a Si adatom. In E12 and E13 the Si adatom is bound to the surface at a dimer-bridge site with energies 0.38 and 0.41 eV relative to E1, respectively. Structure E11 with the two dangling bonds of the broken bridge saturated by H atoms has an energy 1.24 eV higher than E1 and is the least stable structure in group E.

6. Overview

The results of all our calculations are summarized in Fig. 10, in which every stable structure in our survey has been represented by a horizontal bar placed into the figure according to the calculated energy in the vertical direction and degree of PH_3 dissociation (groups A–E) in the horizontal direction. Two important insights can be gained from this arrangement: (1) PH_3 adsorption, progressive dissociation and incorporation leads to increasing energetic stability. Thus the entire process is thermodynamically driven towards incorporation. (2) In each group there exist one or two structures which are substantially more stable than any other in the same group. A thermodynamically favored dissociation path is likely to involve these species. We stress, however, that Fig. 10 does not provide any information about *kinetics* which requires knowledge of the energy barriers between structures. Thus, while a particular structure may be more stable than another, its formation at a given temperature may be prevented on kinetic grounds. Experimentally, P incorporation (evident in the formation of ejected Si adatoms) is not observed[6,12] at temperatures below 650 K, which means that access to the lower energy group E structures in our survey is kinetically hindered. Thus, we focus in the following on the low energy structures in groups A–D as the thermodynamically most likely intermediates seen in STM experiments at room temperature.

B. STM image simulation and assignment of observed features

Having completed our survey of possible PH_3 dissociation products, we are now in a position to assign to particular structures the surface features seen in STM experiments after phosphine dosing. In the following, we will assign three of the most commonly observed STM features: the asymmetric, the centered, and the U-shaped features. In making these assignments, we consider a number of experimental and theoretical aspects: (1) *Simulated STM images* provide the critical information as to whether a given candidate structure has an electronic structure compatible with the experimental appearance. (2) *Energetics*: Low energy structures are thermodynamically more likely to be formed during a dissociation process. Certain structures can be ruled out based on energetics. (3) *Pinning of neighboring dimers*: By calculating the pinning energies E_p (i.e., the energy to flip adjacent dimers from one buckling configuration to the other) for a candidate structure, we can estimate by comparison with kT (0.025 eV at RT) whether neighboring dimers would appear symmetric or buckled in filled state STM images. (4) *Transitions*: Reactions observed in time-resolved STM images provide extremely valuable correlations between two (or more) STM features. Structures assigned to participating STM features must be compatible with the transition. The observed transition can also be expected to proceed from a higher to a lower energy structure.
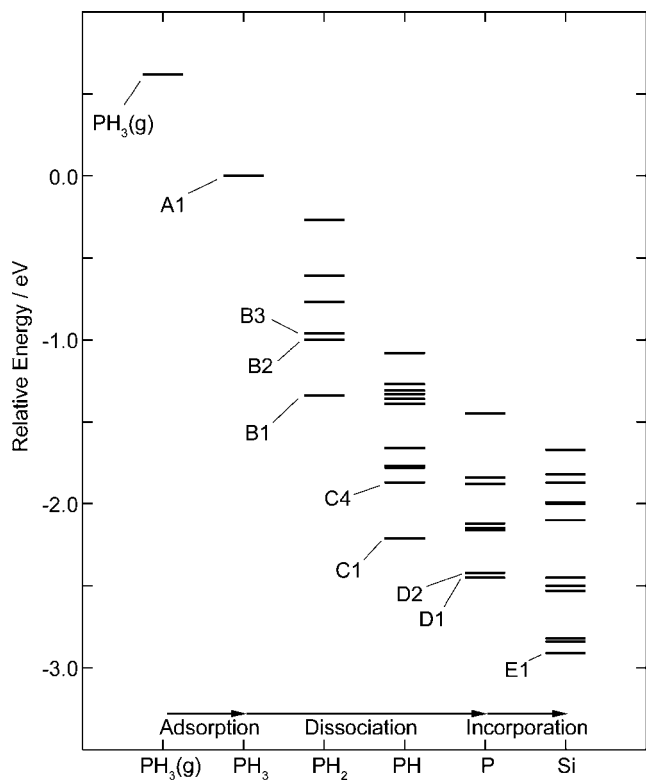
FIG. 10. Overview of energies computed for structures considered in our survey of PH_3 adsorption and dissociation products. Structures are ordered on the horizontal axis according to the PH_x fragment ($x=3,2,1,0$) indicating the degree of dissociation. Low energy structures along the dissociation series from left to right are labeled (A1, B1, C1, etc.).

1. The asymmetric feature

Shown in Fig. 2(b), the asymmetric STM feature is one dimer in width and appears bright on one dimer-end and dim on the other in both filled and empty state images. This STM feature was reported earlier by Schofield *et al.*[5] and assigned as PH_2+H (or structure B1 in our notation). Our results affirm this assignment: Only three structures in our survey, namely A1, B1, and C5, are of single dimer width. Structure C5 can be ruled out because its symmetric structure is incompatible with the asymmetric appearance in experimental STM images. In order to discriminate between A1 and B1 as candidate structures, we show simulated STM images for these two structures in Figs. 11(a) and 11(b), respectively. From these simulations, we expect the A1 structure to appear bright in filled-state on one dimer-end (the site of the bare Si atom, carrying a negative lone pair) and relatively dim (in comparison to surrounding dimers) on both dimer-ends in empty state. The simulation of the B1 feature [Fig. 11(b)] is seen to be bright on the PH_2 side in both filled and empty state images and thus in better agreement with the experimental appearance. A further important clue about the structure of the asymmetric feature is provided by that fact that in the experimental filled-state images [Fig. 2(b)], dimers adjacent to the feature appear symmetric, i.e., not pinned. By comparison of dimer pinning energies E_p of 0.11 and 0.01 eV calculated for structures A1 and B1, respectively, with the
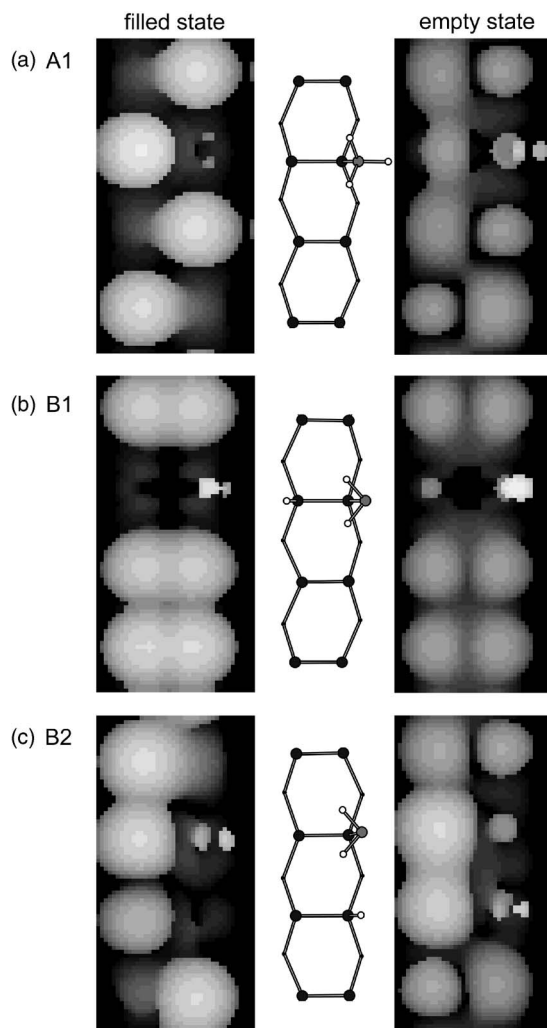
FIG. 11. Simulated STM images for structures (a) A1, (b) B1, and (c) B2. Because structure B1 (unlike A1 and B2) does not pin adjacent free dimers, simulated images of B1 are averaged over the two dimer buckling configurations.

average thermal energy (0.025 eV at RT), we expect structure A1 (unlike structure B1) to strongly pin neighboring defects. Thus the absence of pinning in the experimental image [Fig. 2(b)], combined with the simulated STM images of Fig. 11 conclusively identifies the asymmetric feature as structure B1.

2. The centered feature

Experimental STM images of the centered feature are shown in Fig. 2(a). This feature appears as two dimers wide with a bright centered feature on the first dimer in both filled and empty state and the second dimer appearing dark. This feature has been reported by numerous authors[6,8,9,12] and a variety of interpretations for the central bright feature have been offered; however, none of these works explicitly discuss the adjacent dark dimer.

The bright protrusion in the experimental images points to dimer-bridge and broken-bridge structures of which there are several in our survey: B4, B5, and B6 in group B (structures

PH_2+H), C1–C7 in group C (structure PH+2H), and D5–D9 in the group D (structures P+3H). Since the experimental STM feature is two dimers wide, we can narrow our selection down to structures B4, B5, C1, C6, C7, D7, and D9. Structures B4 and B5 can be ruled out because they exhibit a negative charged lone pair on the second dimer which should appear bright in filled state. The lone pair is also expected to result in strong pinning of nearby free dimers, which is not observed in the experimental image [Fig. 2(a)]. Structures C7 and D7 can be ruled out because they are both asymmetric structures (i.e., the two PH_x bridged dimer-ends are differently substituted) and are both expected to pin neighboring charges due to the formal charge on one dimer-end. This leaves structures C1, C6, and D9; all three plausibly explain the dark dimer as being due to a monohydride which is electronically saturated rendering it dark in both filled and empty state. All three structures are also symmetric with respect to adjacent dimer flipping, and hence, are not pinning. However, as noted previously, C6 is not a minimum and optimizes to C1, while D9 is much higher (0.76 eV) in energy than C1 and can easily relax to C1 by a proton shift. Thus, we assign C1 as the centered feature. The simulated STM images for structure C1 are shown in Fig. 12(a) and are found in excellent agreement with the experimental images [Fig. 2(a)]. The bright appearance in filled state is due to the phosphorus lone-pair orbital, which is raised in energy due to the strain in the three-membered ring.

3. The U-shaped feature

The U-shaped STM feature which is shown in Fig. 2(c) appears as three dimers in width. In filled-state STM images, the feature appears dark except for a moderately bright protrusion on one end of the center dimer, giving this STM feature its characteristic U-shaped appearance. In empty-state images, we see a bright protrusion located on the end-bridge site between two dimers. We note that the dimer that is not involved in the end-bridge appears dark in both filled and empty state, suggesting an electronically saturated dimer, most likely a monohydride.

In our survey there are only a limited number of three-dimer wide end-bridge structures containing a monohydride; namely structures C9, D1, D2, E1, E2, and E7. Of these, D1 and E1 can be ruled out because the center dimer is hydrogen-terminated opposite to the end-bridge and is thus expected to image dark in filled state in contrast to experiment. C9 can be ruled out because neither dimer-end opposite to the end-bridge is H-saturated, thus both are expected to image in at least one of filled and empty state. This leaves us to distinguish between structures D2, E2, and E7. Of these D2 and E2 are the favored contenders on energetic grounds. Both are among the highly probable low energy structures along the dissociation series (Fig. 10).

Simulated STM images for structures D2 and E2 are shown in Figs. 13(b) 13(d), respectively. The relative placement of the brightest protrusions in the simulated D2 filled-state and empty-state images matches the experimental image. The simulated E2 images differ from the observed images in that the silicon on the end-bridge site images brightly in filled-state images whereas the experimental im-
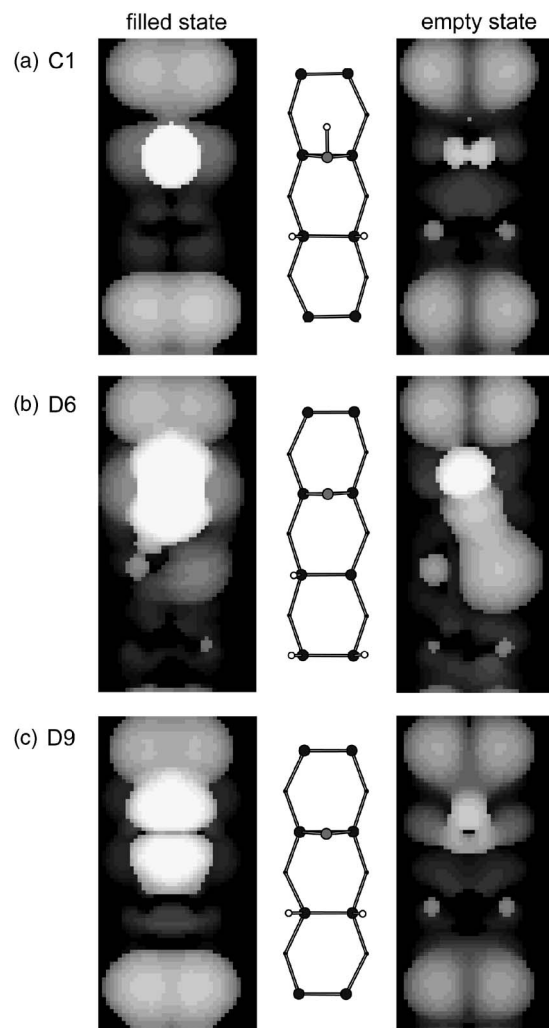
FIG. 12. Simulated STM images for the structures (a) C1, (b) D6, and (c) D9. All three structures do not pin adjacent free dimers and thus the simulated images are averaged over the two buckling configurations of the free dimers.

ages [Fig. 2(c)] show the dimer end site of the middle dimer to be the only bright spot within the three-dimer length of this feature in filled state. Therefore, we assign the U-shaped feature to structure D2.

This assignment is further supported by the observed pinning seen in Fig. 2(c) on one side of the U-shaped feature only. This is seen more clearly in the two additional filled-state STM images in Fig. 14. On the monohydride side no pinning is observed due to symmetry; however, on the other side, pinning is observed and the sense of the pinning is such that the pinned dimer always buckles up on the phosphorus side. This is supported by the calculated pinning energy of $E_p=0.02$ eV in favor of this configuration.

4. Structures not seen in experiment

Additional information about the PH_3 dissociation mechanism can be derived from the low-energy structures in our survey (Fig. 10) for which simulated STM images do not match any of the observed features. In particular, structures
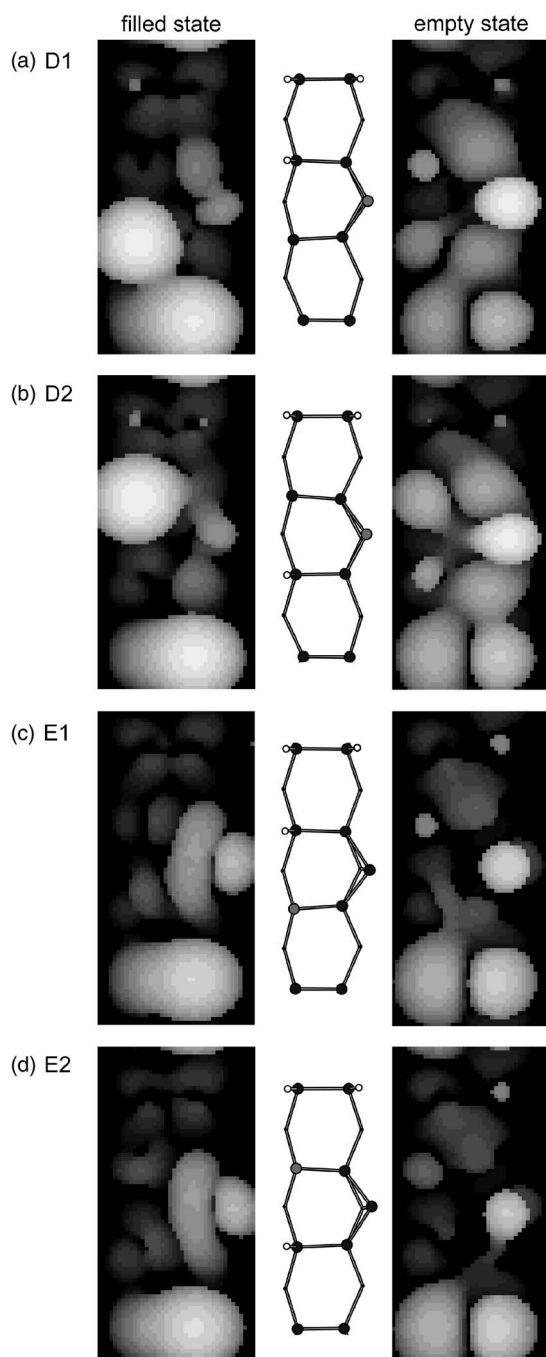
FIG. 13. Simulated STM images for structures (a) D1, (b) D2, (c) E1, and (d) E2.

FIG. 14. (Color online) Two filled-state STM images of the three-dimer wide U-shaped feature showing that free dimers adjacent to the feature on the same dimer row are pinned on one side of the feature only. This is most clearly seen in the left hand image which has higher resolution due to a better STM tip. Images acquired with −1.7 V, 0.1 nA.

A1, D1 and the low energy E structures (E1–E4).

Principally, the nonobservation of a thermodynamically favoured intermediate can be due to one of three kinetic effects: (1) The energy barriers to access a structure could be too high, thus preventing its formation under the given temperature conditions. (2) A structure may have a very low reaction barrier for an onwards reaction to a more stable product, thus making the structure too shortlived to be observable in STM. (3) A structure may not be observable because the formation reaction has to compete with a more favorable reaction to an alternate product; this in effect di-

verts any precursor intermediates before they can transform to the sought structure.

The nonobservation of structure A1 (chemisorbed PH_3) at room temperature is due to a low kinetic barrier to dissociation to PH_2+H (structure B1). This energy barrier was calculated by Miotto *et al.*[23] as 0.39 eV. Transition state barriers calculated by us using the three-dimer $Si_{20}H_{21}$ cluster model, yield barrier energies of 0.77 and 0.54 eV for dissociation to structures B1 and B2, respectively. From these energies, we can estimate the classical room-temperature lifetime of the A1 structure via the Arrhenius equation to be below 0.1 s. In addition, the A1–B1/B2 transitions are proton-shift reactions which are likely to be further accelerated by quantum tunneling through the classical potential energy barrier.[43]

Structure D1 has an energetic stability very similar to the prominently observed U-shaped feature (structure D2); however, we have thus far not found any feature in our experimental STM images in agreement with the simulated STM appearance of D1 shown in Fig. 13(a). The fact that D1 and D2 differ only in the placement of a single H atom provides important clues about the mechanism of D2 formation, which we will discuss further below.

As discussed in the Introduction, formation of the E structures is expected to involve elevated temperatures (650 K).[6,12] Thus, the *E* structures are not seen at room temperature because the transition barriers to P incorporation are too high. The substitution of one dimer-Si atom by a P atom involves multiple bond breakings, namely, two Si-Si backbonds and the dimer-bond. For energetic reasons, this is unlikely to occur in a one-step reaction, but instead involves stable intermediates in which bonds are broken in sequence. Interesting in this context is the elongated backbond in the U-shaped feature (structure D2). The fact that one of the backbonds is already broken should result in a lower activation barrier for an incorporation reaction. Thus D2 appears to be a plausible entry point for P incorporation into a Si dimer.

5. Transition: Asymmetric to centered to U-shaped

Figure 15 shows a time series of three images taken over a period of nine minutes. In this series, an asymmetric feature (B1) can be seen to transform first to a centered feature
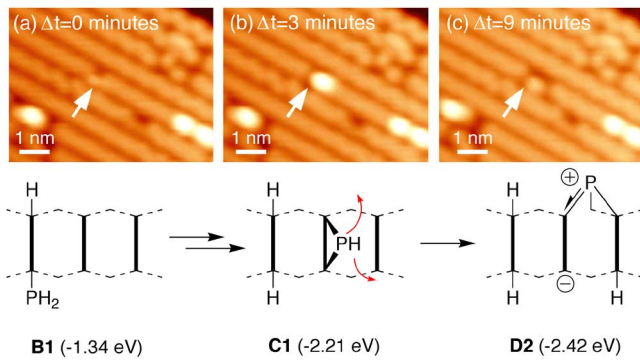
FIG. 15. (Color online) STM time sequence of images showing the progressive dissociation of PH_3 via (a) an asymmetric PH_2 feature (structure B1), (b) the centered C1 and (c), the U-shaped feature D2. The schematic shows the mechanism of dissociation observed in these images.

(C1) and then into a U-shaped feature (D2). This transition has been observed many times in experiment whereas the reverse reaction has never been observed,[26] suggesting that this is an irreversible process. With our structural assignments for the three STM features involved, we understand this process as showing the complete dissociation of a surface adsorbed PH_3 molecule to P+3H (structure D2), with PH_2 and PH species (B1 and C1) as intermediates. Using the calculated relative energies for structures B1, C1, and D2, the transition series is also seen to lead to increasing energetic stability. The B1 structure (PH_2+H on a single dimer) can be seen to stabilize to a centered feature C1 (PH+2H), which undergoes further stabilization to the U-shaped feature D2. This latter step most likely involves a proton shift from the dimer-bridge PH group to the adjacent free dimer leading to the intermediate structure D5 [0.05 eV less stable than C1, see Eq. (3)] followed by a shift of the dimer-bridge P atom to the more stable end-bridge structure D2. An alternative mechanism from C1 to D2, starting with a shift of the PH group from the dimer-bridge to a PH end-bridge position (leading to structure C9), followed by proton shift from the end-bridge PH to a free dimer-end is unlikely for two reasons: (1) The intermediate PH end-bridge structure C9 is 0.88 eV less stable than C1 and thus less likely as an intermediate than D5, and (2), a proton shift from the PH end-bridge is unlikely to have a preference for either of the two dimer-end sites opposite to the end-bridge, resulting in structures D1 and D2 with equal probability. In our STM experiments; however, we have never observed an STM feature consistent with the D1 structure.

The repeated observation of the process shown in Fig. 15 in experiment is consistent with the fact that high-stability intermediates are involved. This affirms, retrospectively, our initial assumption that commonly observed STM features should be among the low energy structure of groups A–D as the thermodynamically most likely intermediates.

IV. DISCUSSION

Let us now consolidate our assignments of three prominent STM features to PH_2+H, PH+2H, P+3H species, and

TABLE V. P-H bond lengths, stretch vibrational frequencies, and infrared intensities calculated for various surface bound species using three-dimer $Si_{21}D_{20}$+PH_3 cluster models. Frequencies have been scaled by 0.971 in calibration to experimental molecular frequencies.

Structure	r(P–H)/Å	δ(P-H)/cm^{-1}	IR Intensity
A1-PH_3^+	1.411	2384	30
	1.408 ($\times 2$)	2411, 2421	2, 3
B1-PH_2 (anti)	1.423 ($\times 2$)	2309, 2319	24,30
-PH_2 (gauche)	1.425 ($\times 2$)	2294, 2305	31,26
C1-PH-	1.427	2279	15

their interconversion seen in STM image sequences, into a more refined mechanism for the thermal decomposition of phosphine on silicon. Before we can do so, we must address the mechanism formulated by Shan *et al.*[20] on the basis of a FTIR vibrational study of the Si(001) surface lightly dosed with PH_3. A particular concern is that these authors conclude that only surface-bound PH_3 and PH_2, but no PH species are formed at room temperature. This is in apparent contradiction with our assignment of prominent STM intermediates as PH_2 and PH species and our nonobservation (at room temperature) of a prominent PH_3 species.

In the FTIR study, two groups of vibrational features in the P-H stretch region are reported: a triplet group of peaks at 2268–2290 cm^{-1} (group I, assigned as PH_3) and a lower group of peaks spanning 2239–2261 cm^{-1} (group II, assigned to PH_2). The authors' assignment of the triplet group to PH_3 was based primarily on the argument that molecularly bound PH_3 is the only species that can give rise to three, closely correlated peaks in the P-H stretch region. The assignment of the group II peaks as due to PH_2 was based on the observation that the group II peaks are associated with thermal decomposition of the species giving rise to the group I peaks. If group I is interpreted as due to PH_3, it follows plausibly that the group II are due to PH_2.

We believe this interpretation of the infrared data should be reconsidered for three reasons. First, structure C1 with its PH species is a natural intermediate in the dissociation from the asymmetric feature (PH_2) to the U-shaped feature (P adatom) on both structural and energetic grounds. Second, the triplet group of peaks is observed for temperatures as high as 450 K, whereas *ab initio* studies predict rapid and complete dissociation into PH_2+H well below room temperature.[23] Third, vibrational frequency calculations performed using the Gaussian cluster model (Table V) show that the signature of surface-bound PH_3 consists of a single high intensity peak and a pair of low intensity peaks about 30 cm^{-1} higher, while the triplet seen in experiments appears as three peaks of similar intensity and even spacing (≈ 11 cm^{-1}).

The vibrational calculations provide an *ansatz* to an alternative interpretation in which the triplet peak may plausibly be assigned to PH_2 rather than PH_3. As seen in Table V, the PH_2 group in the B1 structure has two rotational isomers, i.e.,

$$(4)$$
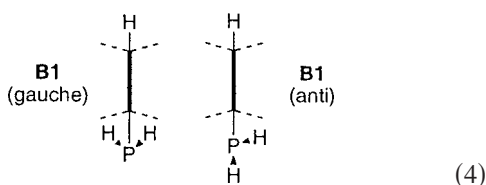
which result in four stretch modes of similar intensity. These four modes would be consistent with a triplet appearance if the conditions of the FTIR experiment convolve the two closely spaced center modes (2305 and 2309 cm^{-1}) into a single peak. We also note that the vibrational signature for the C1 structure is a single peak 15 cm^{-1} below the nearest PH$_2$ peak, and thus is a natural member of the lower group of peaks.

Our summary of a refined dissociation mechanism for PH$_3$ on the Si(001) surface is displayed in Fig. 16. Low-coverage dosing of the Si(001) surface with PH$_3$ leads to the formation of structure A1 containing PH$_3$ molecularly bound to one end of a Si-Si dimer. This species, however, is very short lived at room temperature and dissociates immediately by a proton-shift reaction to structure B1 (PH$_2$+H), which is observed in STM experiments as the asymmetric feature. The lifetime of PH$_2$+H at room temperature is in the order of minutes as revealed in the time sequence of STM images (Fig. 15) leading to structure C1 (PH+2H), a dimer-bridge PH and a monohydride, observed in STM images as the centered feature. The lifetime of the PH+2H centered feature is of the same order as that of the asymmetric feature; over minutes, the dimer-bridge PH dissociates to structure D2 seen as the U-shaped STM feature, containing a phosphorus adatom and three surface bound H atoms. Structure D2 is the end-product of room-temperature dissociation of phosphine. There is no experimental evidence that P adatoms incorporate into the Si(001) surface at room temperature. Indeed, incorporation of P atoms into a surface dimer, that is the formation of heterodimers, does not occur until annealing temperatures of about 650 K are reached.[6,12]

V. CONCLUSION

We have undertaken a comprehensive survey of structures consisting of PH$_x$ species adsorbed on the Si(001) surface, and a partial survey of structures formed by the incorporation of P. We have shown that each step of the phosphine dissociation and phosphorus incorporation process is accompanied by an increase in energetic stability. Through careful consideration of the energetics, and calculation of STM images, we have assigned three of the most commonly observed phosphine dosing features to PH$_2$+H, PH+2H, and P+3H structures, respectively. The asymmetric feature was assigned to structure B1, which is the most stable PH$_2$+H structure. The centered feature was assigned to structure C1, which is the most stable PH+2H structure, and finally, the U-shaped feature was assigned to structure D2, which is the second most stable P+3H structure. Moreover, we have shown that these three structures form a single dissociation pathway, with observed sequences of STM images showing a progression through these stages. Several features commonly seen on the STM surface remain unassigned in this survey.
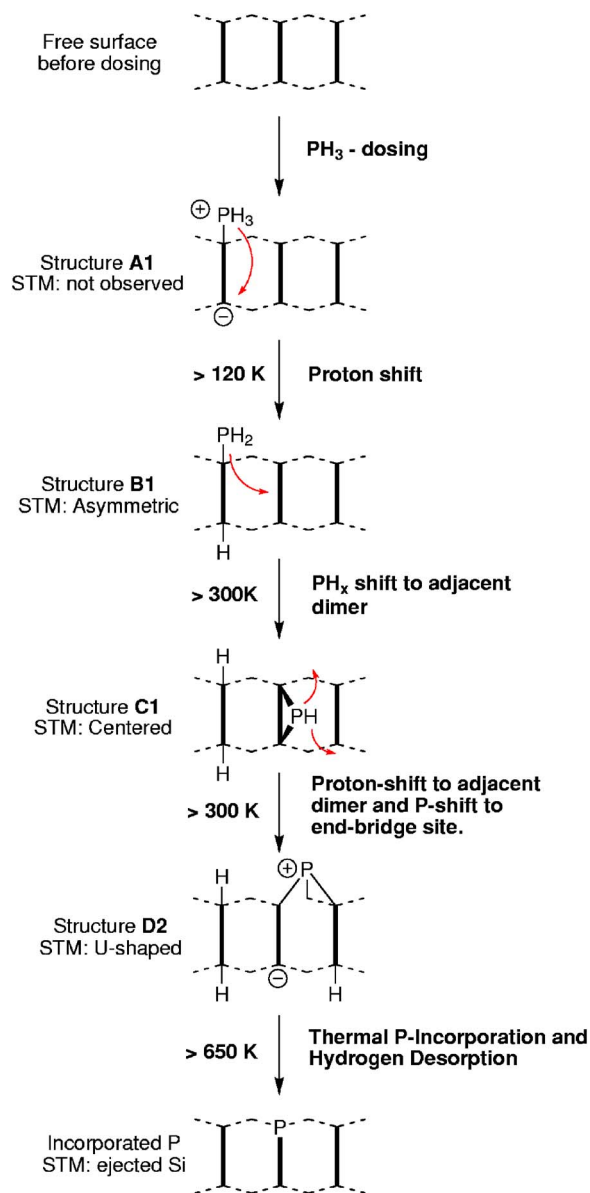
FIG. 16. (Color online) Outline of PH$_3$ dissociation mechanism on the Si(001) surface as revealed in STM images.

Since this survey has only considered structures in which the P and three H atoms remain in close proximity, the possibility of a delocalised dissociation pathway in which the various species are spread across the surface during the dissociation has not been considered. It is highly likely that these alternative dissociation pathways may produce these unassigned features, and further research on this subject is being undertaken.

In conclusion, through the use of several *ab initio* simulation methods we have come to a detailed understanding of the interaction between phosphine and the Si(001) surface. Understanding of this process at the atomic level is vital for a variety of current and future technological applications and provides a model for the study of the chemisorption of other molecules on this surface.

[1] J. R. Tucker and T. C. Shen, Int. J. Circuit Theory Appl. **28**, 553 (2000).

[2] G. L. Snider, A. O. Orlov, I. Amlani, X. Zuo, G. H. Bernstein, C. S. Lent, J. L. Merz, and W. Porod, J. Appl. Phys. **85**, 4283 (1999).

[3] J. L. O'Brien, S. R. Schofield, M. Y. Simmons, R. G. Clark, A. S. Dzurak, N. J. Curson, B. E. Kane, N. S. McAlpine, M. E. Hawley, and G. W. Brown, Phys. Rev. B **64**, 161401(R) (2001).

[4] B. E. Kane, Nature (London) **393**, 133 (1998).

[5] S. R. Schofield, N. J. Curson, M. Y. Simmons, F. J. Ruess, T. Hallam, L. Oberbeck, and R. G. Clark, Phys. Rev. Lett. **91**, 136104 (2003).

[6] Y. Wang, M. J. Bronikowski, and R. J. Hamers, J. Phys. Chem. **98**, 5966 (1994).

[7] Y. Wang, X. Chen, and R. J. Hamers, Phys. Rev. B **50**, 4534 (1994).

[8] L. Kipp, R. D. Bringans, D. K. Biegelsen, J. E. Northrup, A. Garcia, and L.-E. Swartz, Phys. Rev. B **52**, 5843 (1995).

[9] D.-S. Lin, T.-S. Ku, and T.-J. Sheu, Surf. Sci. **424**, 7 (1999).

[10] D.-S. Lin, T.-S. Ku, and R.-P. Chen, Phys. Rev. B **61**, 2799 (2000).

[11] N. J. Curson, S. R. Schofield, M. Y. Simmons, L. Oberbeck, and R. G. Clark, Surf. Sci. **532–535**, 678 (2003).

[12] N. J. Curson, S. R. Schofield, M. Y. Simmons, L. Oberbeck, J. L. O'Brien, and R. G. Clark, Phys. Rev. B **69**, 195303 (2004)

[13] M. L. Yu and B. S. Meyerson, J. Vac. Sci. Technol. A **2**, 446 (1984).

[14] M. L. Yu, D. J. Vitkavage, and B. S. Meyerson, J. Appl. Phys. **59**, 4032 (1986).

[15] M. L. Colaianni, P. J. Chen, and J. T. Yates, Jr., J. Vac. Sci. Technol. A **12**, 2995 (1994).

[16] D. S. Yoo, M. Suemitsu, and N. Miyamoto, J. Appl. Phys. **78**, 4988 (1995).

[17] N. Maity, L.-Q. Xia, S. E. Roadman, and J. R. Engstrom, Surf. Sci. **344**, 203 (1995).

[18] F. Hirose and H. Sakamoto, Surf. Sci. **430**, L540 (1999).

[19] Y. Tsukidate and M. Suemitsu, Appl. Surf. Sci. **151**, 148 (1999).

[20] J. Shan, Y. Wang, and R. J. Hamers, J. Phys. Chem. **100**, 4961 (1996).

[21] H.-W. Tsai and D.-S. Lin, Surf. Sci. **482–485**, 654 (2001).

[22] P.-L. Cao, L.-Q. Lee, J.-J. Dai, and R.-H. Zhou J. Phys.: Condens. Matter **6**, 6103 (1994).

[23] R. Miotto, G. P. Srivastava, and A. C. Ferraz, Phys. Rev. B **63**, 125321 (2001).

[24] R. Miotto, G. P. Srivastava, R. H. Miwa, and A. C. Ferraz, J. Chem. Phys. **114**, 9549 (2001).

[25] R. Miotto, G. P. Srivastava, and A. C. Ferraz, Surf. Sci. **482–485**, 160 (2001).

[26] N. J. Curson, S. R. Schofield, O. Warschkow, N. A. Marks, H. F. Wilson, P. V. Smith, M. W. Radny, D. R. McKenzie, and M. Y. Simmons (unpublished).

[27] H. F. Wilson, O. Warschkow, N. A. Marks, S. R. Schofield, N. J. Curson, P. V. Smith, M. W. Radny, D. R. McKenzie, and M. Y. Simmons, Phys. Rev. Lett. **93**, 226102 (2004)

[28] CPMD Code, J. Hutter, A. Alavi, T. Deutsch, M. Bernasconi, S. Goedecker, D. Marx, M. Tuckerman, and M. Parrinello, MPI fur Festkörperforschung and IBM Zürich Research Laboratory, 1995–2004.

[29] S. Goedecker and C. J. Umrigar, Phys. Rev. A **55**, 1765 (1997).

[30] A. D. Becke, Phys. Rev. A **38**, 3098 (1988).

[31] C. Lee, W. Yang, and R. G. Parr, Phys. Rev. B **37**, 785 (1988).

[32] M. J. Frisch *et al.*, *Gaussian 03*, Revision C.02 (Gaussian, Inc., Wallingford, CT, 2004).

[33] Y. Widjaja and C. B. Musgrave, Surf. Sci. **469**, 9 (2000).

[34] A. D. Becke, J. Chem. Phys. **98**, 1372 (1993).

[35] N. Marzari and D. Vanderbilt, Phys. Rev. B **56**, 12847 (1997).

[36] P. L. Silvestrelli, N. Marzari, D. Vanderbilt, and M. Parinello, Solid State Commun. **107**, 7 (1998).

[37] R. M. Tromp, R. J. Hamers, and J. E. Demuth, Phys. Rev. Lett. **55**, 1303 (1985).

[38] R. A. Wolkow, Phys. Rev. Lett. **68**, 2636 (1992).

[39] H. F. Wilson, N. A. Marks, and D. R. McKenzie, Surf. Sci. **587**, 185 (2005).

[40] J. Tersoff and D. R. Hamann, Phys. Rev. Lett. **50**, 1998 (1983).

[41] J. Tersoff and D. R. Hamann, Phys. Rev. B **31**, 805 (1985).

[42] J. M. Wittbrodt and H. B. Schlegel, J. Phys. Chem. A **103**, 8547 (1999).

[43] Z. K. Smedarchina and M. Z. Zgierski, Int. J. Mol. Sci. **4**, 445 (2003).

[44] R. J. Hamers and Y. Wang, Chem. Rev. (Washington, D.C.) **96**, 1261 (1996).